Observation of Photonic Antichiral Edge States

Peiheng Zhou[1], Gui-Geng Liu[2,3,*] Yihao Yang,[2,3] Yuan-Hang Hu,[1] Sulin Ma[1], Haoran Xue,[2] Qiang Wang[2],
Longjiang Deng,[1,†] and Baile Zhang[2,3,‡]

[1]*National Engineering Research Center of Electromagnetic Radiation Control Materials,*
State Key Laboratory of Electronic Thin Film and Integrated Devices,
University of Electronic Science and Technology of China, Chengdu 610054, China
[2]*Division of Physics and Applied Physics, School of Physical and Mathematical Sciences,*
Nanyang Technological University, 21 Nanyang Link, Singapore 637371, Singapore
[3]*Centre for Disruptive Photonic Technologies, The Photonics Institute, Nanyang Technological University,*
50 Nanyang Avenue, Singapore 639798, Singapore

Chiral edge states are a hallmark feature of two-dimensional topological materials. Such states must propagate along the edges of the bulk either clockwise or counterclockwise, and thus produce oppositely propagating edge states along the two parallel edges of a strip sample. However, recent theories have predicted a counterintuitive picture, where the two edge states at the two parallel strip edges can propagate in the same direction; these anomalous topological edge states are named as antichiral edge states. Here, we report the experimental observation of antichiral edge states in a gyromagnetic photonic crystal. The crystal consists of gyromagnetic cylinders in a honeycomb lattice, with the two triangular sublattices magnetically biased in opposite directions. With microwave measurement, unique properties of antichiral edge states have been observed directly, which include tilted dispersion, chiral-like robust propagation in samples with certain shapes, and 100% scattering into backward bulk states at certain terminations. These results extend and supplement the current understanding of chiral edge states.

Topological materials in two dimensions (2D) are known to exhibit unidirectional, or chiral, edge states at the edges of the bulk [1–7]. For example, in the celebrated Haldane model that exhibits the quantum Hall effect with broken time-reversal symmetry [3], chiral edge states must propagate along the edges either clockwise or counterclockwise, depending on the sign of the Chern number. As a consequence, a typical strip sample must support counterpropagating edge states along its two parallel edges. The time-reversal-invariant quantum spin Hall effect can be treated as a superposition of two copies of the Haldane model, in which the chiral edge states emerge when the spin is fixed [4,5]. Such chiral edge states have not only revolutionized condensed matter physics [1–5], but also opened a new chapter in photonics [6,7] and acoustics [8,9], with applications ranging from one-way waveguides [10–13] and robust optical delay lines [14] to topological lasers [15–18] and photonic circuits [19,20]. For all the above systems, the chiral edge states in a given strip geometry must propagate in opposite directions at the two parallel edges, and the numbers of left- and right-moving edge states must be equal.

Recent theories [21] have predicted another possibility: the edge states at the two parallel edges can propagate in the same direction, as shown in Fig. 1(a), being fully distinctive to conventional chiral edge states, and thus are named as antichiral edge states. These antichiral edge states can occur only in gapless systems, since they need the associated bulk states to propagate in the opposite direction as required by energy conservation. A series of platforms have been theoretically proposed that can potentially realize antichiral edge states, including graphene structures [22,23], exciton polariton strips [24], Heisenberg ferromagnets [25], and gyromagnetic photonic crystals [26]. However, due to the challenging configuration with broken time-reversal symmetry, antichiral edge states have not been observed in reality.

Here, we report the experimental observation of antichiral edge states in a microwave-scale gyromagnetic photonic crystal. Such photonic crystals incorporate gyromagnetic materials to break time-reversal symmetry and have been utilized to demonstrate the photonic chiral edge states [10,11], giving rise to the emerging field of topological photonics [6,7]. We further incorporate on-site modulation of magnetization in such a platform and successfully observe unique properties of antichiral edge states that are still difficult in other platforms.

The challenge to realize antichiral edge states stems from their underlying mechanism that can be described by a modified Haldane model [21] [see Fig. 1(b)]. In the original Haldane model [3], the next-nearest-neighbor coupling picks a nonzero phase that accounts for the magnetic flux
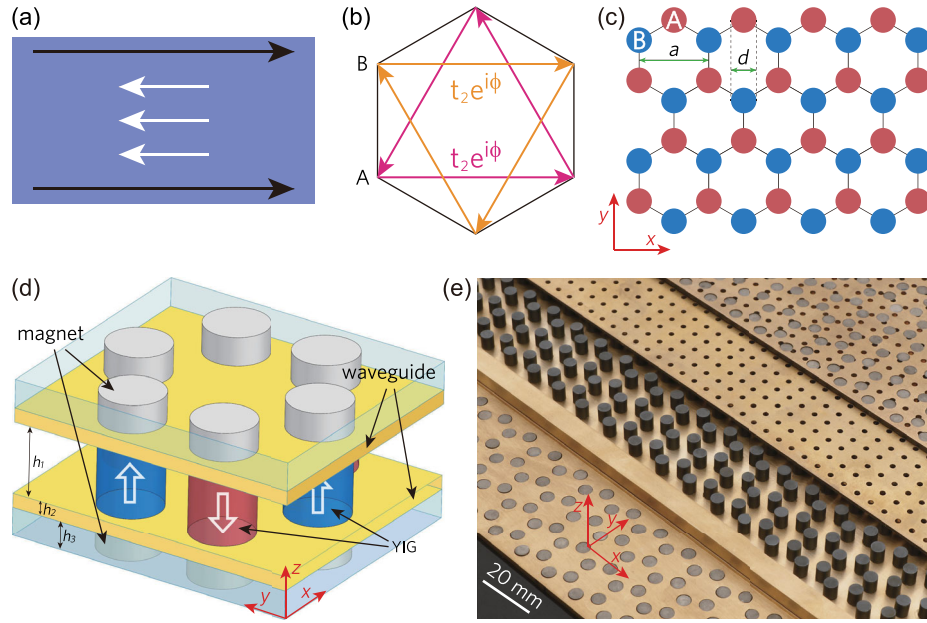
263603-1

FIG. 1. Buildup of antichiral edge states in a gyromagnetic photonic crystal. (a) Conceptual illustration of antichiral edge states that propagate in the same direction, while the bulk states propagate in the opposite direction. (b) The modified Haldane model. The next-nearest-neighbor coupling $t_2 e^{i\varphi}$ directs inversely in sublattices A and B. (c) A photonic honeycomb lattice consisting of gyromagnetic cylinders with identical diameter $d = 4.4$ mm. The lattice constant is $a = 12$ mm. The sublattice A (B) indicated in red (blue) is magnetically biased along the $+$ ($-$) z direction. (d),(e) Design (d) and implementation (e) of the gyromagnetic photonic crystal. The crystal is placed in a parallel-plate copper waveguide with height $h_1 = 5$ mm. The thickness of the waveguide plates is $h_2 = 1$ mm. Permanent magnets of diameter $d = 4.4$ mm and height $h_3 = 2$ mm are embedded in copper plates of the same height and vertically aligned with the YIG cylinders. In (e), the compositional layers are glided two to three lattices away from their edges for photographing.

at the center of a unit cell. However, in the modified Haldane model, the next-nearest-neighbor couplings for different sublattices have opposite signs in phase, meaning that the two sublattices of A and B sites shall "feel" opposite magnetic fluxes.

In photonics, the Haldane model and some variants can be realized in a gyromagnetic photonic crystal under uniform external magnetic fields [10–13,27]. In other words, all gyromagnetic elements are uniformly biased by external magnetic fields. However, for the modified Haldane model, what is necessary is the precise on-site modulation of magnetization. We adopt a honeycomb lattice of gyromagnetic cylinders as schematically illustrated in Fig. 1(c). The cylinders are yttrium iron garnet (YIG) ferrite materials, similar to previous demonstrations inspired by the Haldane model [11–13,27]. However, in the current configuration, the cylinders in the sublattices of A and B sites need to be magnetically biased in opposite directions. This lattice configuration has recently been theoretically studied in Ref. [26], which shows the feasibility of constructing photonic antichiral edge states.

Figure 1(d) shows the schematic of the realization of on-site magnetization modulation. The photo of a concrete sample is shown in Fig. 1(e). The crystal of gyromagnetic cylinders is placed in an air-loaded waveguide composed of two parallel copper plates. On-site magnetization modulation is then enforced by placing samarium cobalt (SmCo)

permanent magnets that sandwich the waveguide with careful designs. The magnets need to be placed exactly above and below the gyromagnetic cylinders. Each gyromagnetic cylinder is sandwiched between a pair of magnets that have the same biasing direction to form a uniform magnetic field in between in the z direction. To fix the positions, the magnets are embedded in two additional copper plates at the top and bottom of the waveguide. By flipping the biasing direction of magnets at neighboring sites, the opposite magnetic fluxes are uniformly applied on the sublattices A and B in the x-y plane, with the same absolute value of 0.043 T in density (see Supplemental Material [28] for the measured magnetic flux distribution).

Note that a square array of small holes is drilled through the top copper plates to allow the insertion of probes for measurement [30]. The thickness of the waveguide plates is essential (1 mm in our case), since it helps to tune the uniform distribution of magnetic fluxes. The following factors play an important role in the success of measurement: the precise control of the lattice site alignment in the entire three-dimensional space, the uniformity of permanent magnets, and the penetration of magnetic fluxes through waveguide plates.

We first probe the dispersion of antichiral edge states. The numerically calculated band dispersion (obtained using finite-element COMSOL Multiphysics) for a strip with zigzag edges is plotted in Fig. 2(a). It can be found that the projected
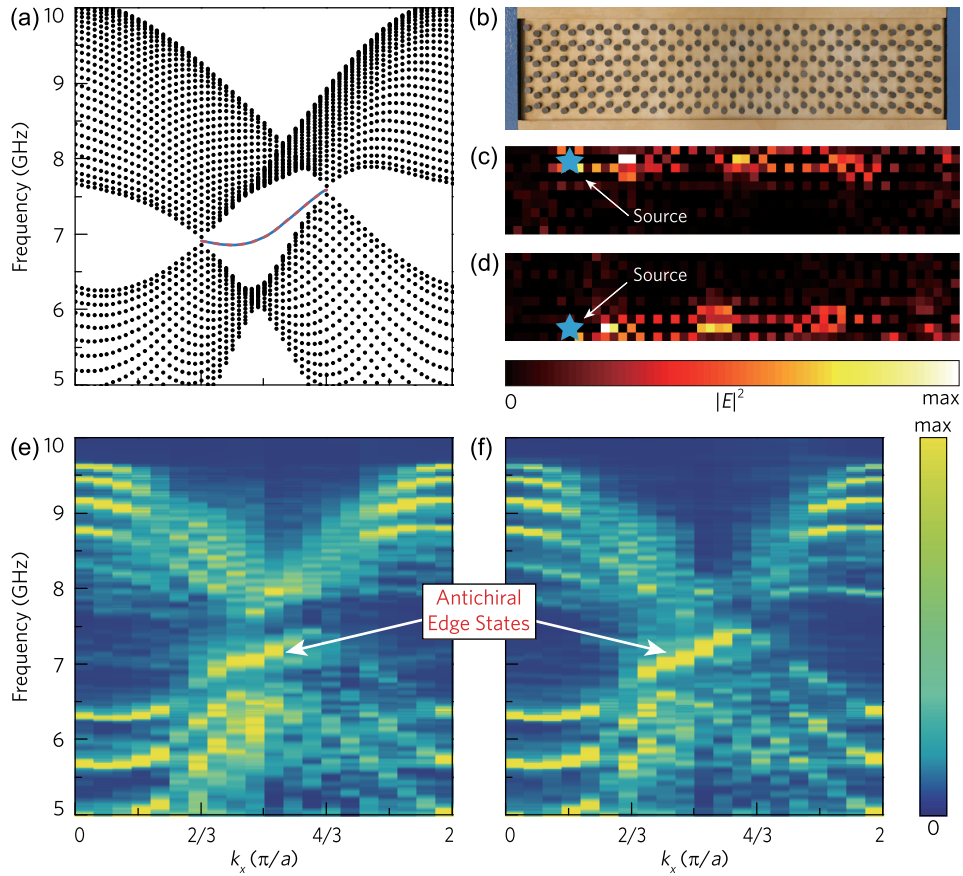
FIG. 2. Observation of antichiral edge states in a strip sample. (a) Numerically calculated band structure for a strip with 15 unit cells in the y direction. The black dots belong to bulk states. (b) Photograph of a strip sample that consists of 5×23 unit cells placed on a copper plate. Copper bars are placed at the upper and lower edges as PEC boundaries. Left and right edges are covered by microwave absorbers (blue). (c),(d) Measured field distribution ($|E|^2$) at 7.3 GHz. The blue star shows the position of the source antenna. (e),(f) Band structure obtained from Fourier transform of the edge states mapped in (c) and (d), respectively.

bulk states of the first and second bands form two degenerate points at $k_x = 2\pi/3a$ (at 6.9 GHz) and $4\pi/3a$ (at 7.5 GHz). These degenerate points are the projections of K' and K Dirac points in the bulk. The corresponding Dirac equations near these Dirac points can be obtained through $\boldsymbol{k} \cdot \boldsymbol{p}$ analysis (see Supplemental Material [28] for details), which shows that, under the oppositely imposed staggered magnetic fluxes, the Dirac points shift only frequencies from K' to K, causing the tilted dispersion of edge states. These edge states are different from the flat edge states in a graphene nanoribbon with zigzag edges [31], because these new edge states both propagate along the $+x$ direction, regardless of the upper or lower edge.

We have constructed a strip sample as shown in Fig. 2(b). Note that the upper (lower) edge corresponds to the A- (B-) type zigzag edge in Fig. 1(c). Copper cladding has been introduced near the upper and lower edges as perfect electric conductor (PEC) boundaries to prevent leakage of electromagnetic waves into the surrounding environment. The left and right edges are covered with microwave absorbers. When a source is located near the

upper or lower edge, the excited edge states will always propagate in the $+x$ direction, as experimentally mapped in Figs. 2(c) and 2(d), respectively. This evidence confirms the existence of antichiral edge states and is fully consistent with the numerical simulation (see Supplemental Material [28]). After applying Fourier transform to the mapped complex field distribution along the edges (see Supplemental Material [28]), we obtain the edge dispersions at the A- and B-type zigzag edges, as indicated in Figs. 2(e) and 2(f), respectively, which match well with the computed band dispersion in Fig. 2(a).

The antichiral edge states are topologically protected in the modified Haldane model [21] (also see Supplemental Material [28] for a discussion on the nontrivial topology in our lattices), spatially separated from the bulk states, and thus can propagate around certain sharp corners without backscattering. Therefore, it is possible to construct carefully designed finite samples where the antichiral edge states can propagate either fully clockwise or fully counterclockwise along all edges, exhibiting chirality similar to that of conventional chiral edge states.
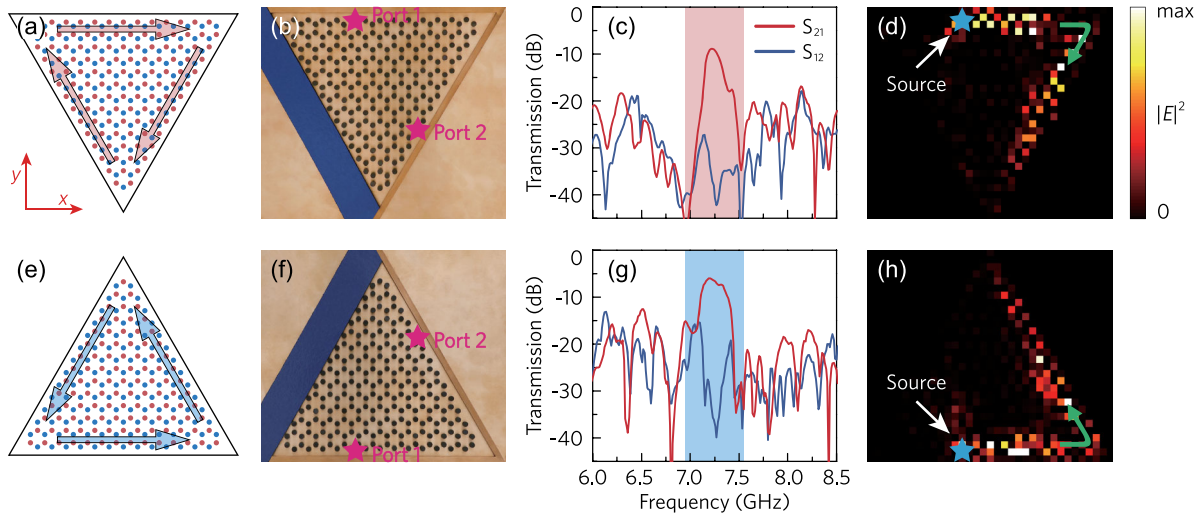
FIG. 3. Robustness of antichiral edge states. (a) Clockwise propagation of antichiral edge states in a downward triangular sample consists of 91 unit cells. All edges are A-type zigzag edges. (b) Photograph of the sample in (a). The sample is wrapped by copper bars and microwave absorber (blue) and placed on a copper plate. (c) Measured transmission. The S_{12} (S_{21}) parameter is measured by placing the source antenna at port 2 (port 1) and detector antenna at port 1 (port 2), as indicated by pink stars in (b). (d) Mapped field distribution ($|E|^2$) for the sample at 7.3 GHz. The blue star shows the position of the source antenna, as the green arrow marks the wave propagation direction. (e) Counterclockwise propagation of antichiral edge states in an upward triangular sample. All edges are B-type zigzag edges. (f) Photograph of the sample in (e). (g),(h) Measured results for the sample in (f), with similar labeling to (c) and (d).

We consider a sample with a downward triangular shape, as illustrated in Fig. 3(a), whose edges are all A-type zigzag edges. According to the above reasoning, the supported edge states can propagate only clockwise along all edges, exhibiting a clockwise chirality. Figure 3(b) shows the photo of a fabricated sample. Since all corners are identical, it is sufficient to demonstrate the robust propagation around one corner. In the measurement, the upper and lower right edges of the sample are confined with copper cladding as PEC boundaries, while the lower left edge is covered with absorbers. A source antenna [labeled as "port 1" in Fig. 3(b)] is placed near the upper edge while a probing antenna [labeled as "port 2" in Fig. 3(b)] collects signal after the sharp corner. As shown in Fig. 3(c), the difference between forward and backward transmissions is larger than 30 dB around 7.3 GHz, indicating the unidirectionality of edge states. Note that this nonreciprocal-transmission frequency window, 6.9–7.5 GHz, is consistent with the numerical simulation in Fig. 2(a). Then, the field distribution at 7.3 GHz inside the sample has been directly mapped point by point, as shown in Fig. 3(d). It can be seen that the edge states are strongly confined to the edges and can propagate robustly across the 60° sharp corner, with no backscattering observed.

Another sample with an upward triangular shape is illustrated in Fig. 3(e). This sample possesses three B-type zigzag edges and, thus, shall support edge states propagating counterclockwise along all edges, showing reversed chirality to the situation in Fig. 3(a). Similarly, we fabricate this sample as in Fig. 3(f). The transmission measurement in Fig. 3(g) and field mapping in Fig. 3(h)

show similar results to those for the downward triangular sample, except the reversed direction of propagation for edge states.

In the original proposal in Ref. [21], antichiral edge states emerge at the two parallel edges of a strip sample that extends to infinity without any termination. As a result, the existence of counterpropagating bulk states that balance the directional antichiral edge states is more for the consideration of energy conservation. Specifically, there is no physical event that can convert antichiral edge states into counterpropagating bulk states. On the other hand, a realistic strip sample shall have certain terminations. It will be interesting to explore the role of such terminations in the energy conversion.

For demonstration purposes, we fabricate a strip sample with a trapezoid termination, whose schematic illustration and real photo are shown in Figs. 4(a) and 4(b), respectively. The upper right 60° corner has no effect on the propagation of antichiral edge states, as we have demonstrated in Fig. 3. That is because the upper and right edges are both A-type zigzag edges. However, the lower right 120° corner can scatter the edge states into backward bulk states. That is because the lower edge is a B-type zigzag edge, which does not match with the other A-type zigzag edges. In the experiment, we place a source near the upper edge to excite the edge states. Field mapping in Fig. 4(c) shows that the edge states can bypass the upper right 60° corner but are fully scattered into bulk states in the backward direction at the lower right 120° corner, without coupling to the lower edge. Note that there is no reflection of edge states observed in the process. Therefore, this
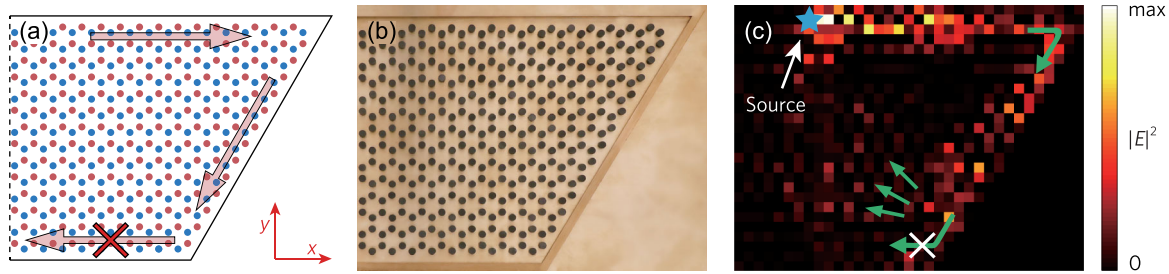
FIG. 4. Conversion of antichiral edge states into bulk states at a termination. (a) Schematic of a strip sample with a trapezoid termination consists of 153 unit cells. (b) Photograph of the sample in (a). The sample is wrapped by copper bars except for the left open edge and placed on a copper plate. (b) Measured field distributions ($|E|^2$) at 7.3 GHz. The blue star shows the position of the source antenna, as the green arrows mark the wave propagation direction.

energy conversion from the edge states to the bulk states is 100% at the lower right 120° corner.

We have thus directly observed the photonic antichiral edge states in a gyromagnetic photonic crystal. The identical propagation directions along two opposite edges are demonstrated by mapping the dispersion as well as the field distribution of photonic antichiral edge states. Another two unique properties, including the chiral-like robust propagation in samples with certain shapes and the 100% scattering into backward bulk states at certain terminations, have been further demonstrated in experiment. Although demonstrated in photonics, these results can be extended to other systems for both fermions and bosons [22–25]. The approach of on-site magnetization modulation may also provide a practical route to some predicted novel phenomena such as the one-way Klein tunneling [32].

Note added.—Recently, we found a recent preprint that reports the observation of antichiral edge states in a circuit network [33].

*guigeng001@e.ntu.edu.sg
†denglj@uestc.edu.cn
‡blzhang@ntu.edu.sg

[1] M. Z. Hasan and C. L. Kane, Colloquium: Topological insulators, Rev. Mod. Phys. **82**, 3045 (2010).

[2] X.-L. Qi and S.-C. Zhang, Topological insulators and superconductors, Rev. Mod. Phys. **83**, 1057 (2011).

[3] F. D. M. Haldane, Model for a Quantum Hall Effect without Landau Levels: Condensed-Matter Realization of the "Parity Anomaly", Phys. Rev. Lett. **61**, 2015 (1988).

[4] C. L. Kane and E. J. Mele, Quantum Spin Hall Effect in Graphene, Phys. Rev. Lett. **95**, 226801 (2005).

[5] B. A. Bernevig and S. C. Zhang, Quantum Spin Hall Effect, Phys. Rev. Lett. **96**, 106802 (2006).

[6] T. Ozawa, H. M. Price, A. Amo, N. Goldman, M. Hafezi, L. Lu, M. C. Rechtsman, D. Schuster, J. Simon, O. Zilberberg, and I. Carusotto, Topological photonics, Rev. Mod. Phys. **91**, 015006 (2019).

[7] A. B. Khanikaev and G. Shvets, Two-dimensional topological photonics, Nat. Photonics **11**, 763 (2017).

[8] Z. Yang, F. Gao, X. Shi, X. Lin, Z. Gao, Y. Chong, and B. Zhang, Topological Acoustics, Phys. Rev. Lett. **114**, 114301 (2015).

[9] G. Ma, M. Xiao, and C. T. Chan, Topological phases in acoustics and mechanical systems, Nat. Rev. Phys. **1**, 281 (2019).

[10] F. D. M. Haldane and S. Raghu, Possible Realization of Directional Optical Waveguides in Photonic Crystals with Broken Time-Reversal Symmetry, Phys. Rev. Lett. **100**, 013904 (2008).

[11] Z. Wang, Y. D. Chong, J. D. Joannopoulos, and M. Soljacic, Observation of unidirectional backscattering-immune topological electromagnetic states, Nature (London) **461**, 772 (2009).

[12] Y. Poo, R.-X. Lin, Z. Wu, Y. Yang, and C. T. Chan, Experimental Realization of Self-Guiding Unidirectional Electromagnetic Edge States, Phys. Rev. Lett. **106**, 093903 (2011).

[13] J.-X. Fu, R.-J. Liu, and Z.-Y. Li, Robust one-way modes in gyromagnetic photonic crystal waveguides with different interfaces, Appl. Phys. Lett. **97**, 041112 (2010).

[14] M. Hafezi, E. A. Demler, M. D. Lukin, and J. M. Taylor, Robust optical delay lines with topological protection, Nat. Phys. **7**, 907 (2011).

[15] Y. Zeng, U. Chattopadhyay, B. Zhu, B. Qiang, J. Li, Y. Jin, L. Li, A. G. Davies, E. H. Linfield, B. Zhang, Y. Chong, and Q. J. Wang, Electrically pumped topological laser with valley edge modes, Nature (London) **578**, 246 (2020).

[16] M. A. Bandres, S. Wittek, G. Harari, M. Parto, J. Ren, M. Segev, D. N. Christodoulides, and M. Khajavikhan, Topological insulator laser: Experiments, Science **359**, eaar4005 (2018).

[17] G. Harari, M. A. Bandres, Y. Lumer, M. C. Rechtsman, Y. D. Chong, M. Khajavikhan, D. N. Christodoulides, and

M. Segev, Topological insulator laser: Theory, Science **359,** eaar4003 (2018).

[18] B. Bahari, A. Ndao, F. Vallini, A. El Amili, Y. Fainman, and B. Kante, Nonreciprocal lasing in topological cavities of arbitrary geometries, Science **358,** 636 (2017).

[19] Y. Yang, Y. Yamagami, X. Yu, P. Pitchappa, J. Webber, B. Zhang, M. Fujita, T. Nagatsuma, and R. Singh, Terahertz topological photonics for on-chip communication, Nat. Photonics **14,** 446 (2020).

[20] S. A. Skirlo, L. Lu, Y. Igarashi, Q. Yan, J. Joannopoulos, and M. SoljačićExperimental Observation of Large Chern Numbers in Photonic Crystals, Phys. Rev. Lett. **115,** 253901 (2015).

[21] E. Colomes and M. Franz, Antichiral Edge States in a Modified Haldane Nanoribbon, Phys. Rev. Lett. **120,** 086603 (2018).

[22] C. Wang, L. Zhang, P. Zhang, J. Song, and Y. Li, Influence of antichiral edge states on Andreev reflection in graphene-superconductor junction, Phys. Rev. B **101,** 045407 (2020).

[23] M. M. Denner, J. L. Lado, and O. Zilberberg, Antichiral states in twisted graphene multilayers, Phys. Rev. Research **2,** 043190 (2020).

[24] S. Mandal, R. Ge, and T. C. H. Liew, Antichiral edge states in an exciton polariton strip, Phys. Rev. B **99,** 115423 (2019).

[25] D. Bhowmick and P. Sengupta, Antichiral edge states in Heisenberg ferromagnet on a honeycomb lattice, Phys. Rev. B **101,** 195133 (2020).

[26] J. Chen, W. Liang, and Z.-Y. Li, Antichiral one-way edge states in a gyromagnetic photonic crystal, Phys. Rev. B **101,** 214102 (2020).

[27] G.-G. Liu, P. Zhou, Y. Yang, H. Xue, X. Ren, X. Lin, H.-X. Sun, L. Bi, Y. Chong, and B. Zhang, Observation of an unpaired photonic Dirac point, Nat. Commun. **11,** 1873 (2020).

[28] See Supplemental Material at http://link.aps.org/supplemental/10.1103/PhysRevLett.125.263603 for the materials and staggered magnetic flux, the Dirac equations, topological protection, simulated edge states in the gyromagnetic photonic crystals, and the Fourier transform method, which includes Ref. [29].

[29] T. Ochiai, Photonic realization of the $(2+1)$-dimensional parity anomaly, Phys. Rev. B **86,** 075152 (2012).

[30] P. Zhou, G.-G. Liu, X. Ren, Y. Yang, H. Xue, L. Bi, L. Deng, Y. Chong, and B. Zhang, Photonic amorphous topological insulator, Light Sci. Appl. **9,** 133 (2020).

[31] E. J. G. Santos, A. Ayuela, and D. Sánchez-Portal, First-principles study of substitutional metal impurities in graphene: Structural, electronic and magnetic properties, New J. Phys. **12,** 053012 (2010).

[32] X. Ni, D. Purtseladze, D. A. Smirnova, A. Slobozhanyuk, A. Alù, and A. B. Khanikaev, Spin- and valley-polarized one-way Klein tunneling in photonic topological insulators, Sci. Adv. **4,** eaap8802 (2018).

[33] Y. Yang, D. Zhu, Z. H. Hang, and Y. D. Chong, Observation of antichiral edge states in a circuit lattice, arXiv:2008.10161.